JACS
JOURNAL OF THE AMERICAN CHEMICAL SOCIETY
Article
pubs.acs.org/JACS

Insights into Thiol−Aromatic Interactions: A Stereoelectronic Basis for S−H/π Interactions

Christina R. Forbes, Sudipta K. Sinha,[‡,§] Himal K. Ganguly,[‡] Shi Bai,* Glenn P. A. Yap,* Sandeep Patel,* and Neal J. Zondlo*

Department of Chemistry and Biochemistry, University of Delaware, Newark, Delaware 19716, United States

Supporting Information

ABSTRACT: Thiols can engage favorably with aromatic rings in S−H/π interactions, within abiological systems and within proteins. However, the underlying bases for S−H/π interactions are not well understood. The crystal structure of Boc-L-4-thiolphenylalanine *tert*-butyl ester revealed crystal organization centered on the interaction of the thiol S−H with the aromatic ring of an adjacent molecule, with a through-space $H_{thiol}\cdots C_{aromatic}$ distance of 2.71 Å, below the 2.90 Å sum of the van der Waals radii of H and C. The nature of this interaction was further examined by DFT calculations, IR spectroscopy, solid-state NMR spectroscopy, and analysis of the Cambridge Structural Database. The S−H/π interaction was found to be driven significantly by favorable molecular orbital interactions, between an aromatic π donor orbital and the S−H σ^* acceptor orbital (a $\pi \rightarrow \sigma^*$ interaction). For comparison, a structural analysis of O−H/π interactions and of cation/π interactions of alkali metal cations with aromatic rings was conducted. Na^+ and K^+ exhibit a significant preference for the centroid of the aromatic ring and distances near the sum of the van der Waals and ionic radii, as expected for predominantly electrostatic interactions. Li^+ deviates substantially from Na^+ and K^+. The S−H/π interaction differs from classical cation/π interactions by the preferential alignment of the S−H σ^* toward the ring carbons and an aromatic π orbital rather than toward the aromatic centroid. These results describe a potentially broadly applicable approach to understanding the interactions of weakly polar bonds with π systems.

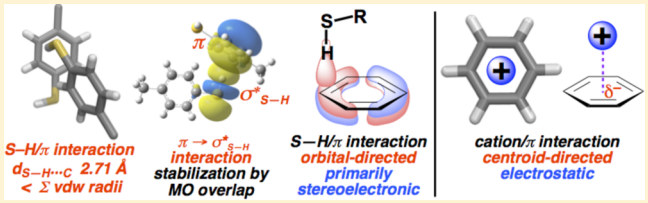

INTRODUCTION

Noncovalent interactions are central to molecular structure, recognition, and assembly. Despite their critical roles, the underlying bases for noncovalent interactions are often not well understood at the fundamental level, precluding accurate assessment of their relative energetic importance and contributions, and making challenging the proper incorporation of these interactions within force fields used for the determination and prediction of structure and dynamics of small molecules, proteins, and higher order complexes.

The thiol (S−H) functional group has versatile roles due to the presence of both hydrogen bond donor and acceptor groups, ready ionization (pK_a typically ∼8), strong nucleophilicity to generate thioethers, and diverse oxidation to disulfide, sulfenic acid, sulfinic acid, sulfonic acid, *S*-nitrosyl, persulfide, sulfonamide, sulfoxide, and sulfone states, among others.[1] The chemical versatility and reactivity of thiols lead to their broad presence in molecular design and recognition, and within biological systems ranging in size from the small-molecule intracellular reductant glutathione to proteins. Thiols can engage in close interactions with aromatic rings, via S−H/π interactions, as one example of a class of sulfur−aromatic interactions.[2] Thiol−aromatic interactions have been observed or implied in diverse contexts, including small molecules, intermolecular assemblies, peptides, and proteins. For example, S−H/π interactions (e.g., Phe−Cys interactions) have been invoked as significant determinants of the stability of the SUMO-1 protein and of certain protein−protein interactions with 7-transmembrane helix receptors.[3] However, the underlying bases for S−H/π interactions are not well understood, due in part to the limited number of structures with hydrogen atoms localized and the limited number of detailed computational investigations outside of the parent H_2S·benzene system (Figure 1), which exhibits a geometry that is not possible for organic thiols (R−S−H, R ≠ H).[2g,h,3a,c,4] Notably, Duan, Smith, and Weaver used *ab initio* calculations (MP2/6-311+G(2d,p)) on a computationally determined MeSH·benzene structure to estimate an interaction energy of 2.6−3.7 kcal mol^{-1} for S−H/π interactions. They also demonstrated, using combined bioinformatics and hybrid computational methods to model the hydrogens in the protein crystal structures, that similar interaction energies were possible within proteins.[4c] However, the underlying bases for these interactions and the specific optimal interaction geometries were not well defined.

More generally, thiol−aromatic interactions are part of a broader class of interactions with aromatic rings, which involve recognition of the negatively charged and electronically tunable aromatic π face.[5] Increased understanding of thiol−aromatic interactions thus could provide insights into fundamental questions in weak polar interactions with aromatic rings. In particular, X−H/π interactions (X = O, N, C, S) are typically

Received: August 11, 2016
Published: January 12, 2017

DOI: 10.1021/jacs.6b08415
J. Am. Chem. Soc. 2017, 139, 1842−1855

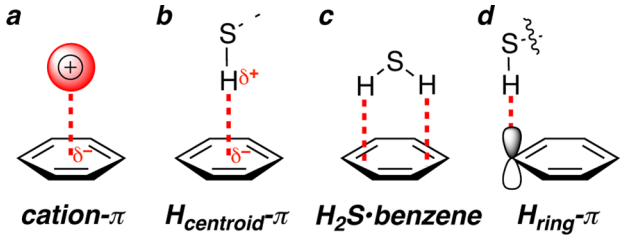

Figure 1. Cation−π interaction and different geometries for S−H/π interactions. (a) Geometry of a cation−π interaction; (b) typical $H_{centroid}$−π structure described for S−H/π interactions, with the H located near the centroid of the aromatic ring to maximize favorable electrostatic interactions with all electrons of the π system; (c) *ab initio* calculated structure of the H_2S·benzene adduct;[2g,h,4a,b] (d) geometry of an orbital-based H_{ring}−π S−H/π interaction, with alignment of the S−H σ^* orbital and an aromatic π orbital. Interactions of type *b* should have minimal dependence on the geometry of the S−H bond but a preference for a position near the centroid of the aromatic ring, to maximize favorable electrostatic interactions with all electrons. In contrast, interactions of type *d* should have a geometric preference for the S−H bond to achieve proper positioning of the S−H σ^* acceptor orbital with the aromatic π donor orbital.

described in significantly electrostatic terms, in analogy to cation/π interactions, in which the partial positive charge (δ^+) on the H can interact favorably with the negatively charged π face, with interactions normally depicted as directed toward the centroid of the aromatic ring, to maximize favorable electrostatic interactions.[2h,4c,6] However, some (but not all) studies have suggested that S−H/π interactions can be similar or even greater in strength than O−H/π or N−H/π interactions, despite the greatly reduced δ^+ on the H in S−H bonds (similar to that of C−H bonds) compared to that in O−H or N−H bonds (with the more electronegative O and N).[2g,h,4c,e] For example, Biswal and Wategaonkar determined from a combination of experiment and theory (on interactions of H_2S, H_2O, NH_3, and CH_4 with both benzene and indole) that the order of X−H/π interaction strengths is S−H > O−H > N−H > C−H, with a specific, significant role of $\pi \rightarrow \sigma^*$ molecular orbital interactions in increasing the strength of S−H/π interactions involving H_2S.[2h] However, these parent compounds can all engage in multidentate interactions of multiple hydrogens with the aromatic rings, which are not possible for alcohols and thiols (R−O−H and R−S−H). Collectively, these results suggest a need for increased understanding of the structure, energetics, and determinants of stability of S−H/π interactions. Herein, we engage in a comprehensive analysis of S−H/π interactions via X-ray crystallography, *ab initio* calculations, IR spectroscopy, solid-state NMR spectroscopy, and analysis of crystallographic databases, comparing and contrasting S−H/π interactions with better understood, but fundamentally different, cation/π interactions.

RESULTS

We recently developed a practical solid-phase approach to the synthesis of peptides containing 4-thiolphenylalanine, the sulfur analogue of tyrosine.[7] This approach involves the synthesis of peptides containing the commercially available amino acid 4-iodophenylalanine, followed by site-selective cross-coupling reaction on solid phase on the fully synthesized peptide with thioacetic acid and copper(I)-phenanthroline. In work directed toward the inclusion of thiolphenylalanine in cysteine-rich disulfide-containing peptides, we alternatively developed a solution-phase approach to this amino acid.[8] The protected Boc-4-iodo-phenylalanine *tert*-butyl ester readily underwent cross-coupling reaction,[7a,9] generating the amino acid with a free thiol upon thiolytic reductive workup. The resultant thiol product, Boc-L-4-thiolphenylalanine *tert*-butyl ester (**1**, Chart 1), crystallized from ethyl acetate/hexanes.

Chart 1. Boc-L-4-thiolphenylalanine *tert*-Butyl Ester (1) and *p*-Thiocresol (2)

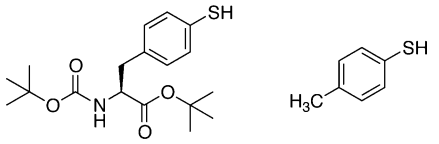

1 **2**

X-ray Crystallography of an S−H/π Interaction. The X-ray crystal structure of **1** (Figure 2) was solved at 0.77 Å resolution, with electron density observed for the thiol hydrogen, allowing the determination of the directionality of the S−H bond vector and hydrogen localization. The crystallographic assembly was partially mediated by hydrogen bonds (2.66 Å H···O distance) between carbamates in adjacent molecules. Examining the thiol, **1** exhibits a typical 99° C−S−H bond angle, with the S−H bond 10° out of the plane of the aromatic ring, and an extended peptide main chain conformation (ϕ, ψ = −140°, +173°; $\chi 1$ = −51° (*g*−)). Interestingly, crystallographic assembly was also mediated by an intermolecular S−H/π interaction, with the S−H directed toward the carbon atoms of the π face of the adjacent aromatic ring. The shortest H···$C_{aromatic}$ distance of 2.71 Å observed is below the sum of the van der Waals radii of H and C (2.90 Å). Sub-van der Waals distances, which are suggestive of orbital-based interactions, have previously been described in S−H/π interactions in a small number of examples both in small molecule crystal structures in the CSD and from protein structures in the PDB.[2k,10] Moreover, X−H bond lengths are typically underestimated by X-ray crystallography, when compared to data from neutron diffraction.[11] When the S−H bond length was normalized to a standard 1.338 Å bond length, the H···$C_{aromatic}$ distance was 2.63 Å, suggestive of a particularly favorable S−H/π interaction.

An additional intriguing feature in the crystal structure was the observation of weak apparent electron density between the thiol hydrogen and the aromatic carbons (Figure 2f). Notably, in the structure of **1**, the thiol S−H interacts with the aromatic ring despite multiple available traditional hydrogen bond acceptors (e.g., ester and carbamate carbonyls, non-carbonyl oxygen lone pairs, and thiol lone pairs), suggesting significant preferential stabilization of thiols via interaction with aromatic rings, consistent with calculations indicating favorable interaction of thiols with aromatic rings.[2g,h,4a,c] Interestingly, cysteine side chains observed in the PDB appear to relatively prefer backbone interactions as a hydrogen-bond acceptor, functioning significantly less frequently as a hydrogen bond donor with carbonyls compared to serine.[12]

IR spectroscopy of an S−H/π Interaction. IR spectroscopy has been used to characterize S−H/π interactions.[2h,10a,c,13] In an interesting example, Boxer and co-workers examined the thiophenol S−H stretching frequency (ν_{S-H}) and intensity in the absence of aromatic cosolvent and in the

DOI: 10.1021/jacs.6b08415
J. Am. Chem. Soc. 2017, 139, 1842−1855

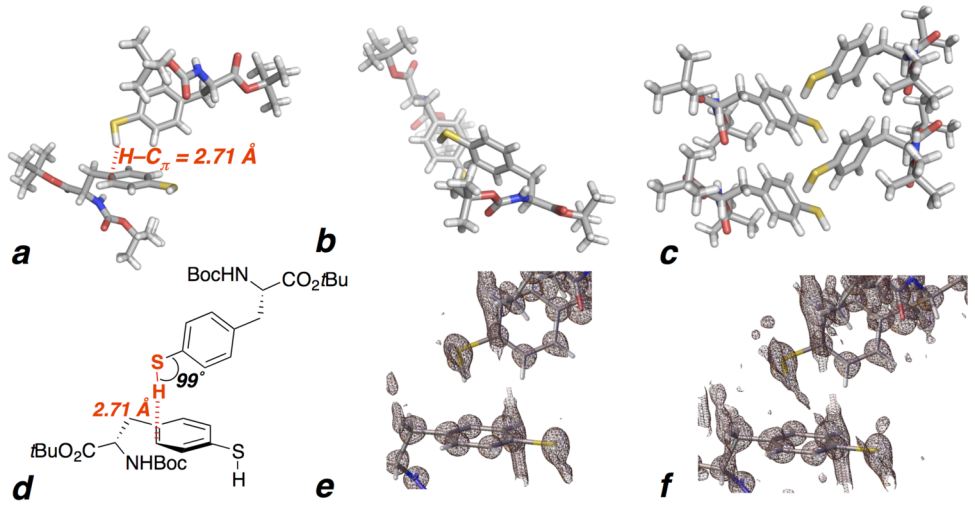

Figure 2. Crystal structure of Boc-L-4-thiolphenylalanine *tert*-butyl ester (**1**). (a,b,d) Two adjacent molecules of **1**, highlighting the interaction of the thiol S−H with the adjacent aromatic ring, with a 2.71 Å H_{thiol}−$C_{aromatic}$ distance between the thiol hydrogen and the nearest aromatic carbon (below the 2.90 Å sum of the van der Waals radii). This electron density-based calculated H_{thiol}−$C_{aromatic}$ distance is based on a S−H bond length of 1.26 ± 0.04 Å, which is within the range of typical thiol S−H bond lengths (average 1.338 Å). The H_{thiol}-centroid distance is 2.90 Å. Gilli and Gilli noted that X-ray diffraction studies typically underestimate X−H bond lengths by 0.1−0.2 Å compared to data from neutron diffraction.[11] If a standardized 1.338 Å S−H bond length is assigned to account for this potential systematic underestimation, as suggested by Gilli and Gilli, then the H_{thiol}−$C_{aromatic}$ distance would be 2.63 Å. The top view (b) shows the vector of the S−H bond directed toward the carbons of the aromatic ring. (c) The S−H/π interaction propagates through the crystal structure. No traditional hydrogen bond is observed to the thiol in the structure. The crystal packing is also mediated by an intermolecular hydrogen bond between the Boc carbamate NH and the carbamate C═O in an adjacent molecule. An intermolecular $H_{aromatic}$−$C_{aromatic}$ interaction is also observed via the aromatic hydrogen adjacent to the thiol (2.84 Å). (e) Electron density map exhibiting the electron density associated with the thiol S−H bond. (f) Electron density map at greater contours showing electron density between the S−H bond and the aromatic ring. In contrast to **1**, the crystal structure of *p*-thiocresol exhibits significant disorder, without ordering at the thiol, likely due to its more planar overall structure.[41]

presence of a series of 11 benzene derivatives.[6b] They observed that the ν_{S-H} red-shifted predictably in solution with increasingly electron-rich aromatic solvents, from non-aromatic CCl_4 (2589 cm^{-1}) to *m*-dichlorobenzene (2581 cm^{-1}) to benzene (2572 cm^{-1}) to the particularly electron-rich hexamethylbenzene (2549 cm^{-1}), indicating a strong aromatic electronic component to interaction of the aromatic ring with the S−H. To further characterize the S−H/π interaction observed crystallographically, the ν_{S-H} of **1** was examined in crystalline form (ν_{S-H} = 2538 cm^{-1}) and in $CHCl_3$ solution (ν_{S-H} = 2585 cm^{-1}) (Figure 3a). These data indicate a 47 cm^{-1} red shift and a > 15-fold increase in the intensity of the S−H stretching frequency in the crystalline form, similar in trend but greater in magnitude than previous observations of S−H/π interactions in crystals.[2h,6b,10a,c] The electronically similar *p*-thiocresol was also examined by IR (Figure 3b), in solution and in the solid-state form, where it forms a disordered crystalline structure with poor localization of the thiol hydrogen (crystal structure details are in the Supporting Information). In $CHCl_3$, the ν_{S-H} of **1** and *p*-thiocresol were identical, as expected. In contrast, the ν_{S-H} of *p*-thiocresol in the solid state exhibited a significantly smaller red shift (ν_{S-H} = 2563 cm^{-1}, $\Delta\nu$ = 22 cm^{-1}) compared to **1** (ν_{S-H} = 2538 cm^{-1}, $\Delta\nu$ = 47 cm^{-1}), consistent with a weaker and less well-defined S−H/π interaction in the *p*-thiocresol crystal. A significant red shift of ν_{S-H} was also observed for **1** and *p*-thiocresol in solvents containing carbonyls (ethyl acetate (ν_{S-H} = 2566−2567 cm^{-1}), acetone (ν_{S-H} = 2558 cm^{-1}), or cosolvent mixtures (10% EtOAc/CCl_4, ν_{S-H} = 2569−2571 cm^{-1}; 10% acetone/CCl_4, ν_{S-H} = 2559−2565 cm^{-1})), with greater intensity of the ν_{S-H} absorbance with an increase in carbonyl cosolvent, consistent with a favorable hydrogen-bonding interaction of the thiol with the carbonyl lone pair or with the carbonyl π system (Figure 3c,d, Table S8).[14] Significant red shifts were also observed in 25% THF/CCl_4 (ν_{S-H} = 2530−2534 cm^{-1}) or 25% methanol/CCl_4 (two bands, ν_{S-H} = 2541−2521 and 2497 cm^{-1}), although these absorbance signals were very broad and of weak intensity. In contrast to the weaker S−H stretching intensities in solution, in the crystalline form of **1**, the S−H stretch was nearly as intense as the carbonyl stretches (Figure 3e,f). In total, the IR data indicate that the S−H/π interaction results in substantial perturbation of the thiol S−H bond, as expected for a molecular orbital-based interaction.

In order to further characterize the nature of the S−H/π interaction, the association of *p*-thiocresol was examined with aromatic compounds with electronically divergent properties, from electron-poor *m*-dichlorobenzene to increasingly electron-rich toluene, 1,3,5-mesitylene, 1-methylindole, and hexamethylbenzene. IR spectroscopy in CCl_4 of the S−H stretching frequency revealed 2 distinct absorbance bands: one non-interacting band associated with free *p*-thiocresol (ν_{S-H} = 2586 cm^{-1}), and one interacting band associated with the S−H/π bound complex (Figure 4). As expected based on prior results, the ν_{S-H} of the interacting band exhibited a red shift whose magnitude was dependent on the electronic properties of the aromatic compound, with hexamethylbenzene (ν_{S-H} = 2549 cm^{-1}) resulting in a 37 cm^{-1} shift in the interacting peak compared to the non-interacting peak. Smaller red shifts were observed for 1-methylindole (ν_{S-H} = 2561 cm^{-1}), mesitylene (ν_{S-H} = 2563 cm^{-1}), toluene (ν_{S-H} = 2571 cm^{-1}), and *m*-dichlorobenzene (ν_{S-H} = 2581 cm^{-1}). Notably, the larger red shift of 1-methylindole compared to toluene suggests stronger S−H/π interactions in proteins with tryptophan than with phenylalanine.

DOI: 10.1021/jacs.6b08415
J. Am. Chem. Soc. 2017, 139, 1842−1855

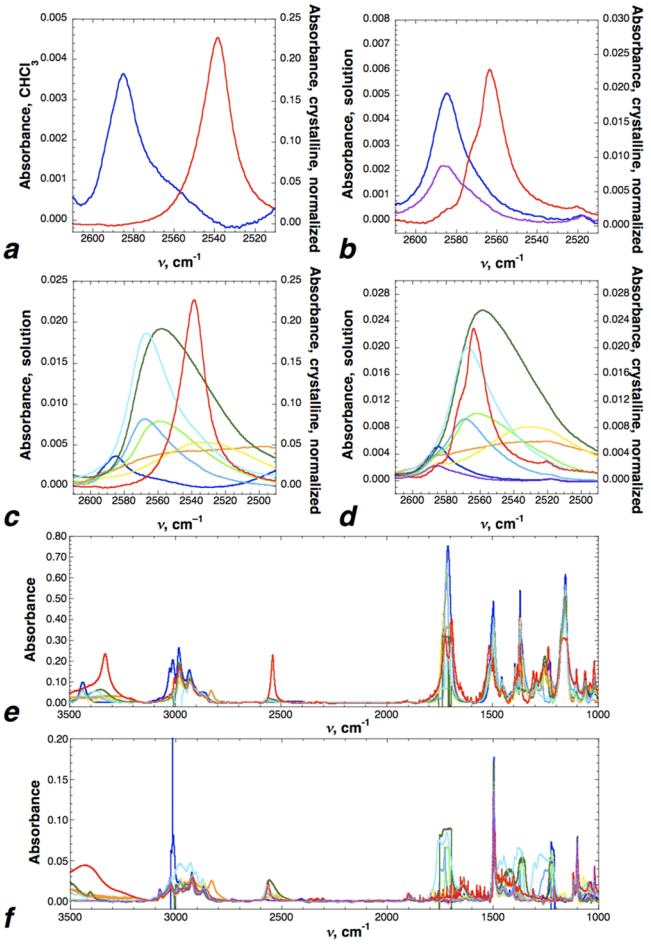

Figure 3. Infrared spectroscopy (S−H stretching region) of **1** and *p*-thiocresol. The left *y*-axis indicates absorbance for molecules (200 mM) in solution. The right *y*-axis indicates the absorbance for crystalline materials, with the crystalline absorbance normalized to the C−H stretching frequency intensity of the molecule in acetone at 2925−2935 cm^{-1}. Note the difference in scales of the left and right *y*-axes in (a)−(d). (a) IR spectra of **1** in $CHCl_3$ (**1**, blue, ν = 2585 cm^{-1}) and in crystalline form (red, ν = 2538 cm^{-1}). (b) IR spectra of *p*-thiocresol in CCl_4 (violet, ν = 2586 cm^{-1}), $CHCl_3$ (blue, ν = 2585 cm^{-1}), and crystalline form (red, ν = 2563 cm^{-1}). (c, d) IR spectra of (c) **1** and (d) *p*-thiocresol in CCl_4 (violet, *p*-thiocresol only), $CHCl_3$ (blue), 25% ethyl acetate in CCl_4 (light blue), ethyl acetate (cyan), 25% acetone in CCl_4 (bright green), acetone (dark green), 25% THF in CCl_4 (yellow), 25% MeOH in CCl_4 (orange), and crystalline form (red). (e, f) Full IR spectra for (e) **1** and (f) *p*-thiocresol. Note the difference in intensity of the S−H stretching frequency in crystalline form versus solution states. Full IR spectra, non-normalized IR spectra, additional solvent data, and tabulation of ν_{max} and intensities for **1** and *p*-thiocresol are in the Supporting Information.

The observation of two distinct IR absorbance bands, representing a free state and a bound state, allowed the determination of the dissociation constants (K_d) and free energies (ΔG) of the *p*-thiocresol complexes with these arenes via concentration-dependent IR spectroscopy. The difference in interaction free energy ($\Delta\Delta G$) of *p*-thiocresol between the most electron-deficient aromatic (*m*-dichlorobenzene) and the more electron-rich aromatic compounds was 1.4−1.8 kcal mol^{-1} ($\Delta\Delta G = \Delta G_{m\text{-dichlorobenzene}} - \Delta G_{aromatic}$), based on the disappearance of the non-interacting peak ($\Delta\Delta G$ = 1.0−1.2 kcal mol^{-1} based on the appearance of the interacting peak, though saturation was not achieved, and thus more error is

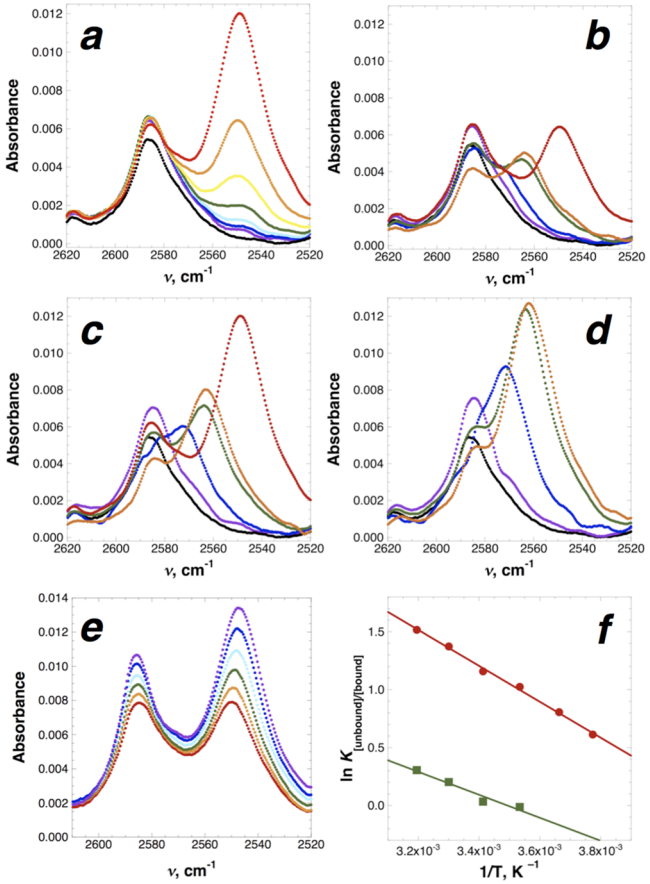

Figure 4. IR-based determination of the thermodynamic parameters of S−H/π interactions between *p*-thiocresol and added aromatic compounds. (a−d) Concentration-dependent IR spectra. Experiments were conducted at room temperature in CCl_4 with 55 mM *p*-thiocresol and 0, 12.5, 25, 50, 100, 200, 400, 800, 1600, and 3200 mM aromatic compound. Experiments with hexamethylbenzene were not conducted at 1600 and 3200 mM due to insufficient solubility. Data represent the average of three independent trials; error bars were omitted for clarity. Data were fit to determine the K_d using a Lorentzian line-fitting algorithm at each concentration.[41] (a) Concentration-dependent IR data indicating the interaction of 55 mM *p*-thiocresol with 0 (black), 12.5 (purple), 25 (blue), 50 (cyan), 100 (green), 200 (yellow), 400 (orange), and 800 (red) mM hexamethylbenzene. The non-interacting peak is at 2586 cm^{-1}, while the interacting peak is at 2549 cm^{-1}. The intensity of the peak at 2586 cm^{-1} includes contributions from the tail of the interacting peak; these effects are quantified in the Lorentzian fitting. (b−d) IR spectra (S−H stretching frequency) indicating S−H/π interactions between *p*-thiocresol and *m*-dichlorobenzene (violet; K_d = 13.5 ± 0.9 M), toluene (blue; K_d = 1.0 ± 0.23 M), mesitylene (green; K_d = 1.0 ± 0.13 M), 1-methylindole (orange; K_d = 0.69 ± 0.11 M), and hexamethylbenzene (red; K_d = 1.3 ± 0.2 M) at (b) 400 mM, (c) 800 mM, and (d) 1600 mM added aromatic. Data on *p*-thiocresol in the absence of an additional aromatic compound are indicated in black. *p*-Thiocresol also exhibits concentration-dependent formation of an additional self-association peak at 2572 cm^{-1} ($K_{self\text{-}association}$ = 0.79 ± 0.12 M). K_d values indicated are based on the disappearance of the non-interacting *p*-thiocresol band; K_d values are higher when based on the appearance of the interacting band and fitting the saturating absorbance and the extinction coefficient of the interacting bands.[41] In addition, the extinction coefficient for the interacting band depends on the added aromatic compound, with higher extinction coefficients for stronger S−H/π interactions (smaller ν_{S-H}).[41] (e) Temperature-dependent change in the IR spectrum of 55 mM *p*-thiocresol in the presence of 400 mM hexamethylbenzene. Experiments were conducted at −8 °C (purple), 0 °C (blue), 10 °C (cyan), 20 °C

DOI: 10.1021/jacs.6b08415
J. Am. Chem. Soc. 2017, 139, 1842−1855

Figure 4. continued

(green), 30 °C (orange), and 40 °C (red). The intensities of both the non-interacting peak at 2586−2587 cm^{-1} and the interacting peak at 2549−2547 cm^{-1} increase with lower temperature. The non-interacting peak exhibits a 1 cm^{-1} blue shift, while the interacting peak exhibits a 2 cm^{-1} red shift, at lower temperature. (f) van't Hoff plot for the interaction of hexamethylbenzene (red circles) and mesitylene (green squares) with *p*-thiocresol. Experiments were conducted with 55 mM *p*-thiocresol and 400 mM added aromatic.

present in these latter numbers, as the maximum absorbance was estimated based on the curve fit; see the Supporting Information for details). These data provide a lower approximation of the favorable energy of an S−H/π interaction, assuming that the interaction with *m*-dichlorobenzene is near the limit of a weak interaction and the one with hexamethylbenzene is indicative of a stronger interaction. Notably, despite the larger IR red shifts in the interacting ν_{S-H} for mesitylene and hexamethylbenzene, their interaction free energies were similar to those of toluene ($\Delta\Delta G$ = 1.4−1.5 kcal mol^{-1}), suggesting that additional factors (such as steric hindrance due to the methyl groups) might be confounding the energetic analysis. Therefore, we also conducted temperature-dependent IR spectroscopy on a subset of aromatics in order to quantify the changes in K_d as a function of temperature and to determine binding thermodynamics via van't Hoff analysis. The *p*-thiocresol·hexamethylbenzene complex exhibited ΔH = −3.0 ± 0.3 kcal mol^{-1} and ΔS = −12.8 ± 1.5 cal mol^{-1} K^{-1}, while the *p*-thiocresol·mesitylene complex exhibited ΔH = −2.2 ± 0.3 kcal mol^{-1} and ΔS = −7.3 ± 1.5 cal mol^{-1} K^{-1}. The ν_{S-H} of the interacting band also exhibited a 2 cm^{-1} red shift at lower temperatures, indicating a more favorable interaction. These data suggest a greater enthalpic component to the S−H/π interaction with the more electron-rich hexamethylbenzene, albeit with greater entropic cost, potentially due to steric effects limiting the geometries accessible for interaction. While the measured free energies and interaction enthalpies and entropies are obviously dependent on additional solution factors, including solvation and potential competition with aromatic−aromatic interactions, these experimentally determined energies are consistent with prior computational and experimental analyses of the strengths of S−H/π interaction and suggest that S−H/π interactions can make substantial energetic contributions to the stabilities of structures and at the interfaces of complexes.

S−H/π Interactions Exhibit through-Space Scalar Coupling. To further characterize the nature of the S−H/π interaction, we examined the structure of **1** and *p*-thiocresol by ^{1}H and ^{13}C solid-state magic-angle spinning (MAS) NMR and compared these data to solution ^{13}C NMR data ($CDCl_3$ and CD_3OD). ^{13}C−^{1}H 2D FSLG HETCOR experiments on crystalline **1** revealed that the thiol hydrogen exhibited strong coupling with the *ortho* or *meta* carbon, but not with the nearer *para* (S-bound) carbon, of the aromatic ring (Figure 5), at both shorter (Figure S87a) and longer (Figure 5a) mixing times, consistent with the close interaction of the thiol hydrogen with these carbon atoms that was observed crystallographically. In *p*-thiocresol, two thiol hydrogens were observed by ^{1}H MAS NMR, one with strong coupling to the aromatic carbons and one with weak coupling, consistent with two thiol hydrogen environments observed in the crystalline phase. Notably, *intermolecular* scalar coupling has previously been observed in

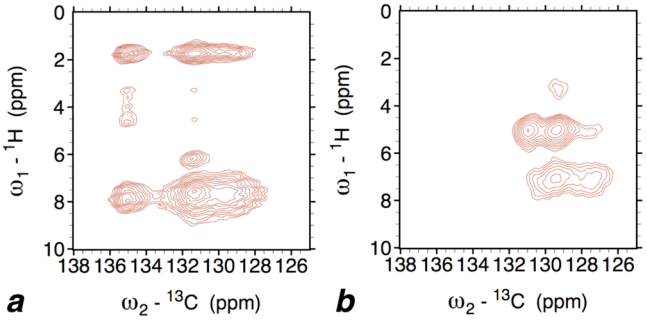

Figure 5. ^{13}C−^{1}H HETCOR solid-state magic-angle spinning (MAS) NMR spectra (aromatic carbon correlations) of crystalline **1** (a, 1000 μs mixing time) and crystalline *p*-thiocresol **2** (b, 300 μs mixing time). (a) The thiol hydrogen (6.2 ppm) exhibits coupling to the *ortho* or *meta* carbon (131 ppm), as is observed close in space crystallographically, but not to the *para* (129 ppm, closest covalent through-bond distance) or *ipso* (135 ppm) carbons. This coupling is also observed at 300 μs mixing time (Figure S87a). (b) *p*-Thiocresol exhibits two thiol hydrogens, an interacting thiol (5.0 ppm, strongly coupled to the aromatic carbons, particularly the *ortho* and *meta* carbons crystallographically suggested to interact with the thiol) and a non-interacting thiol (3.2 ppm, weakly coupled to the aromatic carbons), consistent with the disordered crystal structure (Figure S112). Both hydrogen resonances disappeared in the 1-D solid-state NMR spectrum after deuterium exchange (Figure S92).

C−H/π interactions in proteins in solution and in the solid state by HETCOR experiments, consistent with through-space coupling occurring via favorable orbital overlap.[15]

DFT Calculations on an S−H/π Interaction. In typical crystal structures, the geometry and even the presence of an S−H/π interaction is often difficult to identify due to the low electron density at the hydrogen atoms, a problem that is particularly acute when trying to identify S−H/π interactions in proteins.[2c,k,4a,c,6c,10d] Thus, different surveys of the PDB have yielded wildly varying estimates of the number of cysteine−aromatic S−H/π interactions. This lack of structural data has also complicated calculations of the energetics and determinants of stabilization of S−H/π interactions, particularly outside of the well-studied H_2S·benzene dimer, whose bidentate mode of interaction (Figure 1c) is not possible for typical thiols.[2g,h,4a,b,16] Therefore, calculations on a crystallographically determined non-H_2S S−H/π interaction geometry (i.e., an R−S−H/π thiol/aromatic interaction) could provide substantial insights applicable to understanding diverse S−H/π interactions. A truncated key structure derived from the crystal structure of **1**, representing a *p*-thiocresol dimer with the geometry observed in **1** (Figure 6), was examined via *ab initio* calculations (B3LYP and MP2 methods, each with 6-311+G-(2d,p) and aug-cc-pVDZ basis sets) followed by natural bond orbital (NBO) analysis.[17] These data indicate significant orbital overlap between the aromatic π donor orbital and the S−H σ^* acceptor orbital, with substantial energetic stabilization (1.52 kcal mol^{-1} by MP2/aug-cc-pVDZ) derived almost entirely (1.45 kcal mol^{-1}) from overlap of these frontier molecular orbitals, as had been observed by Biswal and Wategaonkar in describing the stabilization of the H_2S·benzene dimer.[2h] Calculations (MP2/aug-cc-pVDZ) with NBO analysis were also repeated using a normalized 1.338 Å S−H bond length, which results in a 2.63 Å $H_{thiol}\cdots C_{aromatic}$ distance (Figure 7). NBO analysis at this more likely S−H bond length indicated 1.91 kcal mol^{-1} in stabilization energy due to the $\pi \rightarrow \sigma^*$ molecular orbital interaction shown (overlap between this

DOI: 10.1021/jacs.6b08415
J. Am. Chem. Soc. 2017, 139, 1842−1855

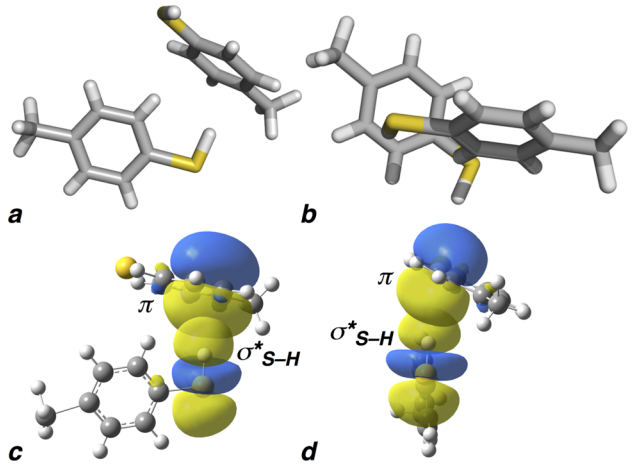

Figure 6. Density functional theory (DFT) calculations with natural bond orbital (NBO) analysis of the minimalist *p*-thiocresol dimer. (a, b) Structure of *p*-thiocresol dimer used for calculations, derived from the geometry observed crystallographically in **1**. (c, d) Two views of the energetically favorable geometric in-phase molecular orbital overlap between the aromatic π donor orbital and the S–H σ^* acceptor orbital. Calculations were based on the crystallographically determined 1.26 Å S–H bond length.

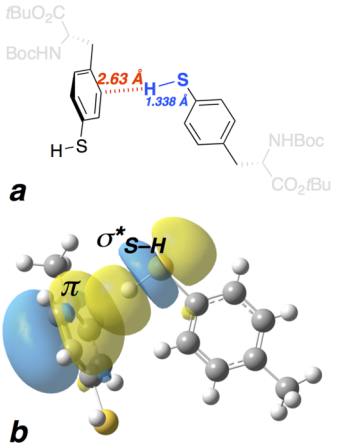

Figure 7. Computational analysis of the S–H/π interaction with the S–H bond length normalized to a standard 1.338 Å. (a) Representation of the crystal structure of **1** that was used to generate the *p*-thiocresol model employed in calculations. All atom positions except those of the thiol hydrogens are identical to those in Figure 6. (b) NBO analysis of the calculation (MP2/aug-cc-pVDZ) of the *p*-thiocresol dimer with the normalized S–H bond length. The shaded yellow area indicates the extent of orbital overlap between the π donor and σ^* acceptor orbitals, which is greater than in Figure 6c,d due to the closer approach of the thiol.

$\pi_{aromatic}$ and the σ^*_{S-H}). Notably, the crystallographically observed alignment of the thiol, with the hydrogen nearer to the carbons of the aromatic ring (as opposed to the centroid) and the S–H bond pointing toward the bonds of the ring, promotes the near-maximal overlap of these molecular orbitals. This proposed stereoelectronic basis for the S–H/π interaction also explains the substantially sub-van der Waals H···C distance observed in the crystal, which increases the extent of $\pi \rightarrow \sigma^*$ orbital overlap and thus the extent of stabilization. The substantial calculated energetic stabilization is also consistent with the unusual observation of electron density between the thiol hydrogen and the aromatic carbon. These calculations also emphasize the large antibonding orbitals associated with bonds to sulfur and the special abilities of these strong acceptor σ^* orbitals in molecular recognition.[2e,j,18]

Typical X–H/π interactions, as well as classical hydrogen bonds, are described predominantly in electrostatic and induced dipole/polarization terms, here with the negatively charged π face interacting with the partial positive charge on the hydrogen.[6b,19] The calculated *p*-thiocresol dimer contains two thiols, one of which interacts with an aromatic ring and the other of which is non-interacting. Comparison of the non-interacting and π-interacting thiols thus provides insight into the role of electrostatics in the S–H/π interaction. The charges of the non-interacting H_{thiol} and S were calculated using CHELPG as +0.21 and −0.29, respectively, consistent with the small difference in electronegativity of H compared to S. Notably, this partial positive charge is similar to that of the aromatic hydrogens (+0.09 to +0.16) and suggests only a modest electrostatic driving force for S–H/π interactions, particularly in water, which exhibits substantially more charged hydrogens than those in thiols. The calculated charges of the π-interacting H_{thiol} and S were +0.21 and −0.34. These data indicate a small change in polarization and a small induced dipole interaction in the presence of an S–H/π interaction. Nonetheless, these data still indicate a very modest electrostatic basis for an S–H/π interaction, particularly in water. Combined with NBO analysis, these data suggest that the primary driving force for the S–H/π interaction is a favorable stereoelectronic effect (HOMO/LUMO-like molecular orbital interaction) driven by the π donor and the strong S–H σ^* acceptor.

DFT calculations (B3LYP/cc-pVTZ) were also employed to examine the dependence of S–H bond length and interaction with the aromatic ring on the ν_{S-H} (Table S19). These calculations indicated that increasing the S–H bond length led to a decrease in ν_{S-H}, with $\nu_{S-H} \approx 2580$ cm^{-1} (similar to the experimental value in $CHCl_3$) corresponding to a 1.36 Å S–H bond length; an identical S–H bond length and similar ν_{S-H} (2560 cm^{-1}) were recently calculated for geometry-optimized tri-*tert*-butoxysilanethiol.[14c] In contrast, for the crystallographically determined S–H bond length of 1.261 Å, the calculated ν_{S-H} was ∼3320 cm^{-1}, substantially greater than that observed experimentally. Using the TPSSh method with the cc-pVTZ basis set, the data indicated that the aromatic-interacting S–H has a 16 cm^{-1} lower frequency and ∼20-fold greater intensity than the non-interacting S–H at the identical bond length. Combined, these data support the use of standardized S–H bond lengths in crystal structures and indicate that the smaller S–H IR frequencies observed in S–H/π interactions could result from longer S–H bonds, from direct interaction of the thiol with the aromatic ring, or from a combination thereof.

Analysis of S–H/π Interactions in the CSD. In order to understand the generality of the geometry observed in the crystal structure of **1**, and explained via *ab initio* calculations, we conducted a search of the Cambridge Structural Database (CSD) for other S–H/π interactions (Figure 8).[20] This search found previously described examples of S–H/π interactions[2j,10a–c,16b] and identified 45 total structures (62 total thiols) with H···Cπ distances below the sum of the van der Waals radii of H and C (<2.90 Å) (complete list of structures and distances in Table S1). Distances below 2.5 Å were observed in multiple structures, with the shortest H···Cπ distance 2.20 Å. Interestingly, similar to the structure of **1**, in many of these structures, the S–H/π interaction is observed despite the presence of traditional hydrogen bond acceptors for

DOI: 10.1021/jacs.6b08415
J. Am. Chem. Soc. 2017, 139, 1842–1855

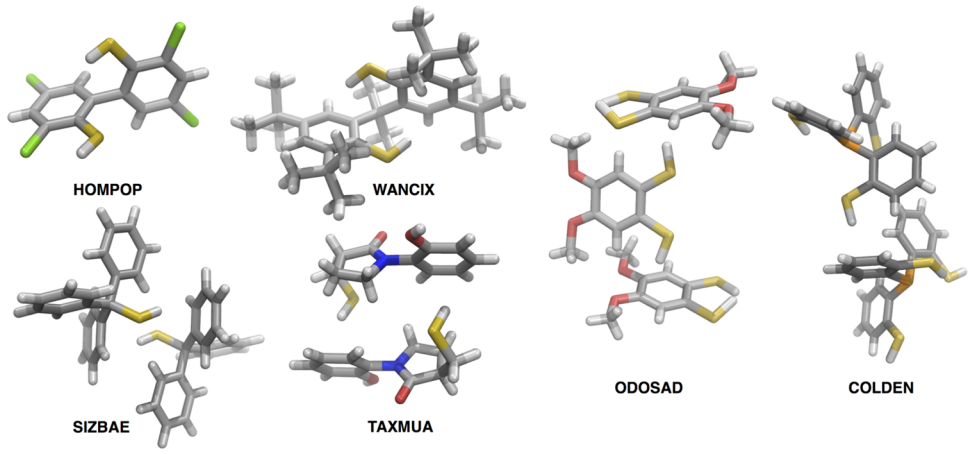

Figure 8. S−H/π interactions in the CSD, based on a search for C/Si−S−H···Cπ distances ≤2.90 Å. Selected structures are shown, with the CSD code indicated. Minimum H_{thiol}−$C_{aromatic}$ distances are 2.48 Å (HOMPOP),[42] 2.20 Å (WANCIX),[43] 2.47 and 2.70 Å (ODOSAD),[44] 2.49 Å (COLDEN),[45] 2.79 Å (SIZBAE),[46] and 2.78 Å (TAXMUA).[10a] The distances for each structure are based on the hydrogen positions in the crystal structure CIF files, whose hydrogens for these examples are explicitly described in the original publications. The minimum H_{thiol}−$C_{aromatic}$ distances after standardization of S−H bond lengths to 1.338 Å are 2.33 Å, 2.15 Å, 2.45 Å, 2.62 Å, 2.54 Å, 2.94 Å, and 2.81 Å, respectively.

the thiol. Several interesting examples are indicated in Figure 8. *ortho*-Benzenedithiol was observed in multiple structures to exhibit S−H/π interactions preferentially over interactions with the thiol as the hydrogen bond acceptor (e.g., ODOSAD). In addition, several examples exhibited S−H/π interactions preferentially over thiol interactions with carbonyls. While crystal packing obviously influences the relative interactions that are observed, these data strongly suggest that S−H/π interactions can be central elements in molecular assembly, consistent with calculations suggesting energies of S−H/π interactions to be comparable to other well-described noncovalent interactions.[2h]

The structures were further analyzed geometrically to determine the distance of the thiol hydrogen from the nearest aromatic carbon (d_{H-Cmin}), from the centroid of the ring ($d_{H-centroid}$), from the plane of the ring (d_{plane}), and from the centroid in the parallel plane (r), which indicates the distance of the hydrogen from the centroid when projected orthogonally onto the plane of the ring (Figure 9; analysis with S−H bond lengths normalized to 1.338 Å is in Figure 10 and the Supporting Information). In general, these structures exhibit geometries that are most likely to place the thiol hydrogen approximately above the aromatic carbons, nearer the π orbitals of the ring, with little evidence of the hydrogen near the centroid of the ring (i.e., $d_{H-Cmin} < d_{H-centroid}$), in the manner typically described for cation−π interactions to maximize favorable electrostatics. Notably, in contrast to the simple representation in Figure 1d, the S−H/π interaction geometries are heterogeneous with regard to the relationship of the S−H bond vector to the plane of the aromatic ring, potentially partly due to the diffuse and extended nature of S−H σ* orbitals. However, the closest interactions are aligned with the S−H σ* acceptor orbital directed toward the aromatic π donor orbital. This carbon-directed (as opposed to centroid-directed) geometry for S−H/π interactions has also previously been noted in two limited surveys of the CSD and PDB, though no explanation was given for this apparent preference.[10d,16b] The observation of a local maximum of H_{thiol} located ∼1.4 Å radially from the centroid of the aromatic ring is strongly suggestive of a favorable nature for this geometry, which would allow the greatest extent of orbital overlap between the π and the σ* orbitals, as was suggested in calculations to be particularly energetically favorable. In contrast, at H···C distances significantly greater than the sum of the van der Waals radii, this geometric preference was not observed, consistent with the stabilization of an S−H/π interaction being highly dependent on appropriate orbital overlap.

Comparison of S−H/π Interactions to Cation/π and O−H/π Interactions in the CSD. To further understand the differences between cation/π and S−H/π interaction geometries, we analyzed all cation−π interactions involving simple Li^+, Na^+, and K^+ alkali metals interacting with aromatic rings in the CSD.[21] Alkali cation/π interactions represent an electrostatic limiting case for interactions with aromatic rings and thus were used as an initial reference point for a purely electrostatic interaction. The differences between the geometries of the purely electrostatic cation/π interaction and the S−H/π interaction could therefore provide insights into the nature of the latter.

While cation/π interactions have been thoroughly characterized in diverse contexts, including extensively computationally, there has not to our knowledge been a recent large-scale analysis of the geometries of simple (alkali metal) cation/π interactions in the CSD.[5d,22] Based on the geometric cutoffs employed ($r \leq 3.0$ Å from the aromatic centroid, $d_{plane} \leq 1.25 \times$ the sum of the van der Waals (C) and ionic (M^+) radii), we found 23 structures with Li^+/π interactions (43 Li^+), 66 structures with Na^+/π interactions (84 Na^+), and 196 structures with K^+/π interactions (365 K^+). Consistent with theoretical and prior crystallographic descriptions of cation/π interactions, we observed that a significant fraction of Na^+/π and K^+/π interactions exhibited geometries with the cation near the centroid of the aromatic ring and with the cation located at approximately the sum of the van der Waals and ionic radii from the aromatic ring. In 23% of Na^+/π and 45% of K^+/π interactions ($r \leq 3.0$ Å), the cation was located nearer to the centroid of the aromatic ring than to any of the carbons of the ring (statistical likelihood if randomly distributed: $(0.7)^2/(3.0)^2$ = 5.4%), with a significant maximum observed for centroid-directed interactions. Moreover, the further the distance of the cation from the plane of the aromatic ring (larger d_{plane}), the weaker its geometric preference for the centroid of the ring,

DOI: 10.1021/jacs.6b08415
J. Am. Chem. Soc. 2017, 139, 1842−1855

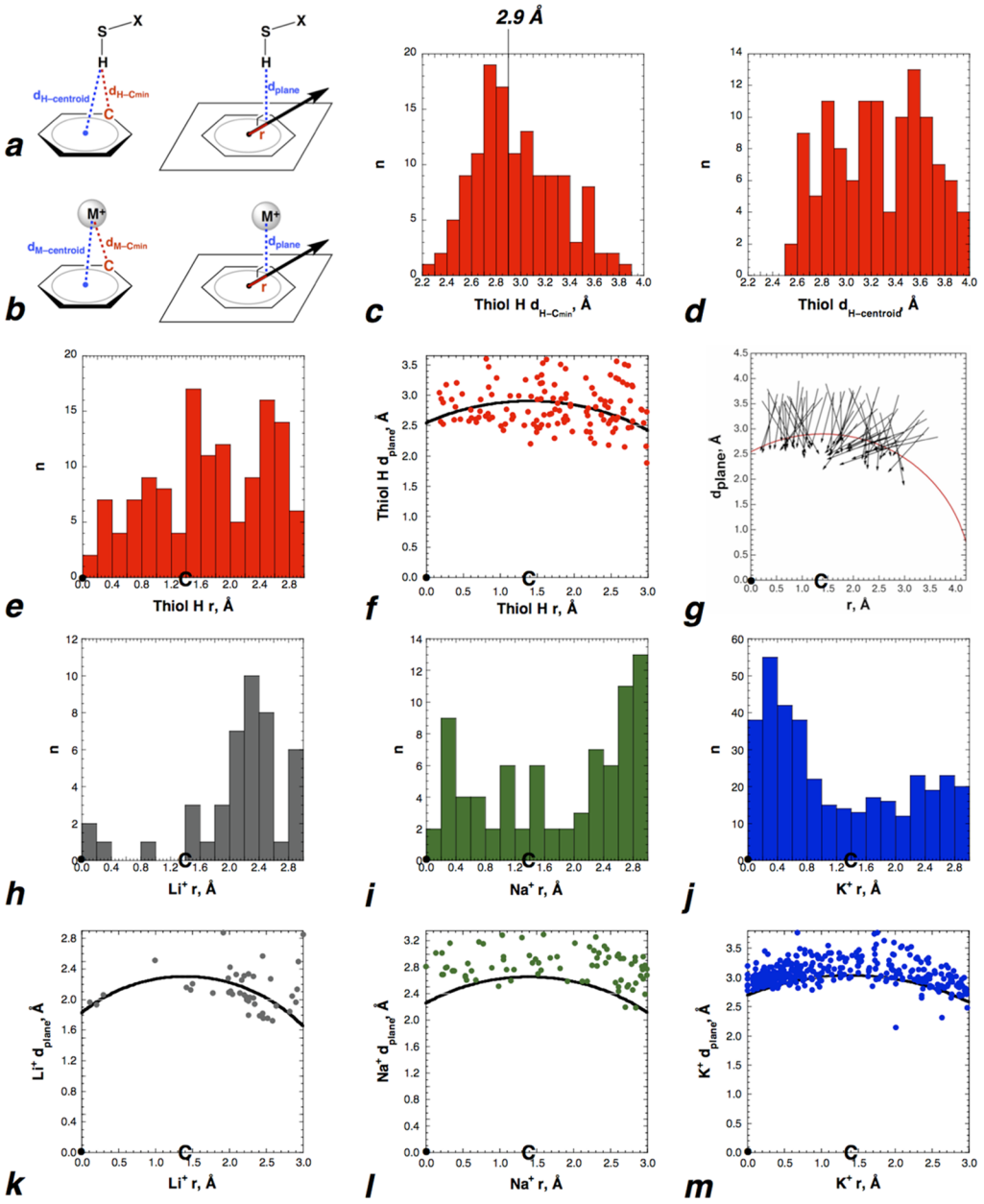

Figure 9. Analysis of S−H/π interactions and alkali cation/π interactions, geometries, and distances in the Cambridge Structural Database (CSD). (a) Definitions of distances measured in S−H/π interactions: d_{H-Cmin} = distance between the thiol H and the nearest aromatic carbon (shortest $H_{thiol}-C_{aromatic}$ distance); $d_{H-centroid}$ = distance between the thiol H and the centroid of the aromatic ring; d_{plane} = distance from the thiol H to the plane of the ring, via projection at 90° to the plane of the ring; r = distance of the thiol H, projected onto the plane of the ring, from the centroid of the ring; • indicates the location of the centroid of the aromatic ring. **C** indicates the location of the carbons of the aromatic ring (1.40 Å from the centroid). Similar definitions were applied to the distances of the thiol sulfur (Supporting Information) and the analyzed cations from the ring and ring components. Full data sets from CSD searches are in Tables S1−S5. (b) Definition of distances in cation/π interactions. Definitions are as in panel a, with M = Li^+, Na^+, or K^+. Search parameters for panels a and b include all S−H and M^+ with $r \leq 3.0$ Å and with $d_{plane} \leq 1.25 \times \sum$(van der Waals or ionic radii of C and H or M^+). (c, d, e) Histograms of d_{H-Cmin}, $d_{H-centroid}$, and r for all thiols in this analysis. In contrast to expectations for a purely electrostatic interaction, hydrogens are on average closer to the carbons of the ring than to the centroid, and a significant percentage of the hydrogens are within the 2.9 Å sum of the van der Waals radii of H and C. (f) Comparison of d_{plane} as a function of distance from the centroid of the ring. The 2.90 Å sum of the C and H van der Waals radii, indicated by the line (a radius of 2.90 Å centered on the aromatic C, which is 1.40 Å from the centroid of the ring), results in shorter "allowed" distances at the centroid of the ring than directly over the carbons of the ring. The centroid of the aromatic ring thus has two geometric advantages for a purely electrostatic interaction: the ability to interact with the entire electron cloud of the aromatic ring, and the ability to have a closer interaction with the ring without repulsive interactions. Despite these advantages, there are few thiol hydrogens near the centroid of the ring. (g) S → H bond vectors for all thiols in which d_{H-Cmin} was ≤2.90 Å. Analysis in panels c−g was based on the S−H bond lengths in the CIF files (mean S−H bond length 1.20 ± 0.12 Å; mean X−S−H bond angle 102.8° ± 8.2°; median X−S−H bond angle 100.3°). Full analysis of thiols in the CSD with all S−H bond lengths normalized to 1.338 Å is in the Supporting Information (Table S2, Figures S104−S105, S107). Additional analysis is in the Supporting Information. (h−m) Li^+, Na^+, and K^+ cation/π interactions in the CSD as a function of distance from the centroid (r) and distance from the plane (d_{plane}). The line indicates the sum of the van der Waals and ionic radii of C and the

DOI: 10.1021/jacs.6b08415
J. Am. Chem. Soc. 2017, 139, 1842−1855

Figure 9. continued

indicated cation. K^+ interactions in the CSD closely resemble the classical description of a cation/π interaction, with a preference for location of the cation near the centroid of the aromatic and distances at or somewhat greater than the sum of the van der Waals and ionic radii.

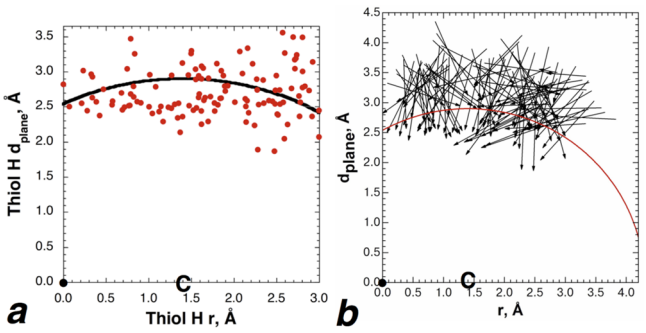

Figure 10. Analysis of S−H/π interactions with the S−H bond length normalized to 1.338 Å. Definitions are as in Figure 9. The 2.90 Å sum of the C and H van der Waals radii is indicated by the line (a radius of 2.90 Å centered on the aromatic C, which is 1.40 Å from the centroid (•) of the ring). (a) Comparison of the distance of the thiol hydrogen from the plane of the ring (d_{plane}) as a function of aromatic plane-projected distance from the centroid of the ring. (b) S → H bond vectors for all thiols.

consistent with expectations for a primarily electrostatic interaction. Interestingly, Li^+/π interactions deviated quite substantially from the trends for Na^+ and K^+, with distances substantially below the sum of the van der Waals radii and a greater tendency for interaction toward the π orbitals instead of the centroid, as had been described previously in a more limited analysis by Kochi and co-workers.[22e] While the Li^+ cation is substantially smaller and harder than Na^+ or K^+, allowing more favorable electrostatic π interactions, as observed previously in the gas phase and in calculations, the geometry and distances may also allow the possibility of interaction between the aromatic π orbital and the empty 2s orbital of Li^+. Notably, Kochi and co-workers also observed the involvement of molecular orbital interactions of aromatic systems with the larger alkali metal cations Rb^+ and Cs^+, including puckering at interacting carbons, as η^1- or η^2-interactions.[22e] Indeed, the geometries observed for S−H/π interactions are more analogous to cation/π interactions with transition metals, such as Ag^+ or Au^+, which typically exhibit η^1- or η^2-interaction geometries, consistent with substantial identified covalent character and a significant molecular orbital component to the interactions.[23] In sum, these data suggest that pure, "classical" electrostatic cation/π interactions, with the cation interacting at the centroid of the aromatic ring, as depicted in Figure 1a, are only fully applicable within the alkali metals to Na^+ and K^+. These observations collectively also are consistent with the possibility of significant molecular orbital components to other interactions with aromatic rings, particularly when only a weak electrostatic component is involved.

O−H/π interactions have been previously examined and compared to S−H/π interactions via experimental and computational techniques.[2g,h,4e,6a,b,19] While purely electrostatic approaches to understanding X−H/π interactions suggest that the significantly greater δ^+ on H in an alcohol should lead to stronger O−H/π interactions than S−H/π interactions, both experimental and computational data suggest similar overall interaction energies. To understand the similarities and differences between these interactions, a search of highly ordered structures (R < 0.05) in the CSD was conducted for alcohols interacting with aromatic rings (Figure 11). The search

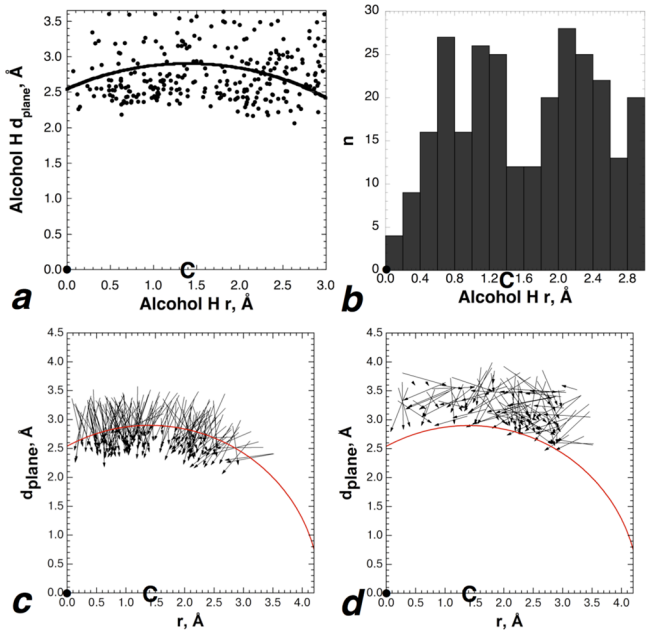

Figure 11. Analysis of O−H/π interactions in the CSD for alcohols not engaged in traditional hydrogen bonds nor bound to metals. Definitions are as in Figure 9. The 2.90 Å sum of the C and H van der Waals radii is indicated by the line (a radius of 2.90 Å centered on the aromatic C, which is 1.40 Å from the centroid (•) of the ring). (a) Comparison of distance of the alcohol hydrogen from the plane of the ring (d_{plane}) as a function of the aromatic plane-projected distance from the centroid of the ring. (b) Distance of the alcohol hydrogen from the centroid when projected onto the plane of the aromatic ring. (c, d) O → H bond vectors for alcohols with hydrogen−carbon distances (c) less than or (d) greater than the 2.90 Å sum of the van der Waals radii of hydrogen and carbon.

results were then further analyzed to separate alcohols that were engaged with nearby classical hydrogen-bonding groups or metals from those that were near the aromatic ring but not near other hydrogen-bonding groups, in order to focus on structures more likely to represent "purely" O−H/π interactions (see the Supporting Information for details and for additional analysis of both data sets). The resultant structures were analyzed as described above for S−H/π and cation/π interactions. These data indicated that 83% of alcohols located near aromatic rings (1725 alcohols) were engaged in hydrogen bonds or interactions with metals, while 17% of these alcohols (290 alcohols) could be considered examples of canonical O−H/π interactions. In contrast, 87% of thiols near aromatic rings were interacting primarily with the aromatic ring, consistent with extensive data that alcohols engage more favorably in hydrogen bonds than do thiols and suggesting that aromatic groups compete effectively with traditional hydrogen bond acceptors for interactions with thiols. Analysis of the alcohols engaged in O−H/π interactions revealed no

DOI: 10.1021/jacs.6b08415
J. Am. Chem. Soc. 2017, 139, 1842−1855

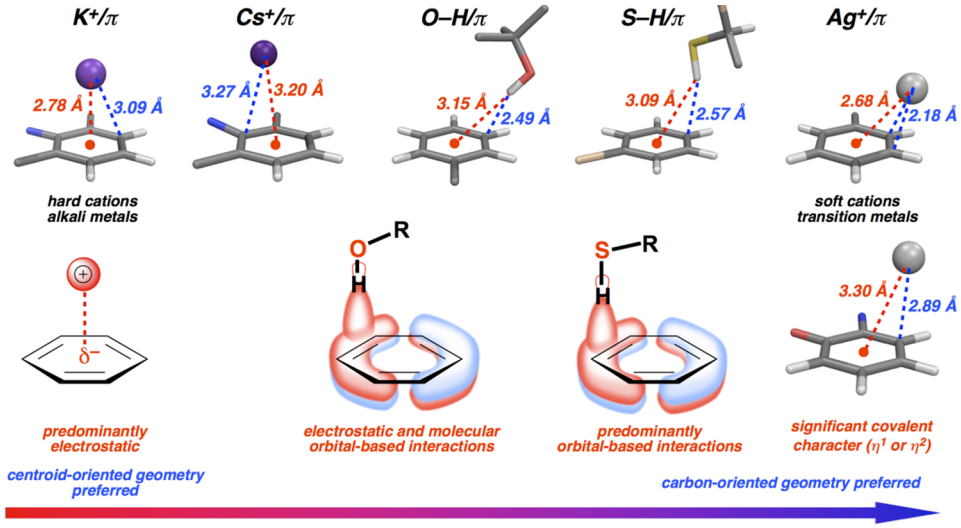

Figure 12. Crystallographically observed representative geometries of cation/π, O–H/π, and S–H/π interactions. Interaction geometries represent a continuum of electrostatic and molecular orbital (covalent)-based effects. Classical (alkali metal) cation/π interactions are centroid-directed (η^6-like) with geometries dictated by electrostatic effects. In contrast, transition metal cation/π interactions often exhibit substantial covalent character (η^1-, η^2-, or η^3-interactions), in addition to electrostatic effects. O–H/π and S–H/π interactions similarly exhibit a combination of electrostatic and molecular orbital-based (covalent-like) effects, with a greater likelihood for location near the carbons (π molecular orbitals) and for H···C distances below the sum of the van der Waals radii than for K^+/π interactions. Structures from left to right (CSD codes): YOLDAG, VIKDOK, AHOSAT, KOYJIT, PUXNUR, TITKUE; atoms not involved in the aromatic interaction have been removed for clarity.[23h,47] An analysis of Ag^+/π interactions in the CSD is included in the Supporting Information.

preference for the centroid of the aromatic ring, in contrast to cation/π interactions. Numerous very close contacts (substantially below the sum of the van der Waals radii of H and C) were observed, indicating substantial potential strength of O–H/π interactions.

Notably, in contrast to S–H/π interactions, here no strong radial preference (i.e., no special preference to be near the C═C bonds) was observed. The computationally determined lowest energy conformation of the phenol/benzene O–H/π interaction includes association of the hydrogen with the center of a carbon–carbon bond,[6a,24] with an H···C distance of 2.5–2.6 Å, consistent with a role for a molecular orbital interaction ($\pi \rightarrow \sigma^*_{O-H}$) in addition to electrostatics.[25] However, this preference appears to be weaker for O–H/π interactions than for S–H/π interactions. Indeed, Biswal and Wategaonkar determined by NBO analysis that H_2O·indole exhibits 1.6 kcal mol^{-1} less orbital interaction energy than H_2S·indole.[2h] Moreover, for O–H/π interactions outside the sum of the van der Waals radii of H and C, there is essentially no directional preference for the O–H bond vector, suggesting a purely electrostatic interaction in this longer distance regime. In contrast, some directionality still exists even for S–H bonds beyond the sum of the van der Waals radii, consistent with the large σ^*_{S-H} and the more energetically favorable nature of this orbital–orbital interaction. Consistent with these interpretations, Boxer and co-workers observed a strong linear correlation between electric field and IR frequency shift for phenol·aromatic complexes. However, very substantial deviation from linearity was observed in this attempted correlation for thiophenol·arene complexes.[6a,b] Collectively, these results suggest a greater role for electrostatics in the strength of O–H/π interactions, but a relatively greater role for molecular orbital overlap in the strength of S–H/π interactions. More broadly, these data are consistent with geometries and bases for interactions with aromatic rings representing a continuum of electrostatic and molecular orbital-based effects (Figure 12), from predominantly electrostatic interactions of π systems with the alkali metal K^+, which results in a preference for a centroid-oriented geometry, to interactions that also include covalent character, resulting in a carbon-oriented (π molecular orbital-oriented) geometry, as is frequently observed for transition metals and for S–H/π interactions.

DISCUSSION

We have described the comprehensive analysis of the S–H/π interaction, via X-ray structural determination of a crystal assembled via S–H/π interactions, IR spectroscopic analysis to identify changes in the S–H bond as a result of interaction with the aromatic ring, solid-state MAS NMR to identify interactions in the solid state, *ab initio* calculations based on the crystallographically observed geometry to identify the underlying nature of the S–H/π interaction, and large-scale analysis of crystallographically observed S–H/π interactions in the CSD and the comparison and contrast of these interactions with the classical cation/π interactions that are often used to describe them. In this work, the data suggest a fundamental molecular orbital interaction, between an aromatic π donor orbital and the S–H σ^* acceptor orbital, to be the major stabilizing force in an S–H/π interaction.[2h]

Despite the inherent chemical similarity of oxygen and sulfur, third row elements have 3s/3p-derived orbitals that extend further from the nucleus than 2s/2p-derived orbitals. In addition, repulsive interactions with electrons in 2s/2p-derived non-bonding orbitals change the inherent geometries of bonds to sulfur compared to bonds to oxygen. Thus, while water and aliphatic alcohols exhibit bonds with sp^3-like geometries (~109° angles), and phenols exhibit sp^2-like geometries (i.e., C–O–H bond angle ~120°), bonds to sulfur are more typically ~90°–105°.[2j] Similarly, in the structure of **1**, we observed a 99° C–S–H bond angle, which is different from that of tyrosine (~120°) and points to the unique structural

DOI: 10.1021/jacs.6b08415
J. Am. Chem. Soc. 2017, 139, 1842–1855

possibilities of thiolphenylalanine, in addition to its access to diverse oxidative modifications.[7,8,26]

An additional interaction possible with third row (and lower) elements takes advantage of the larger antibonding orbitals and the lower, more accessible energies associated with these orbitals. Thus, in contrast to oxygen, sulfur (via the σ^* of S−H and S−C bonds) can interact favorably with lone pairs (n), leading to structural organization via n → σ^* interactions, whereas oxygen is more typically repulsive in this context due to unfavorable electrostatics.[2j] Similarly, methionine residues interact favorably with aromatic rings, via alignment of methionine C−S σ^* with the aromatic π system.[2e,f,18,27] These interactions are also analogous to halogen bonding, in which lone pairs can interact favorably with the "sigma hole" of C−halogen bonds, through both favorable electrostatic and orbital-based interactions, with observed halogen bond strength iodides > bromides > chlorides ≫ fluorides.[28]

S−H/π interactions have been described or proposed in small molecule and protein contexts, though the identification and underlying basis of S−H/π interactions have been challenging to understand due to a lack of hydrogen localization (especially in proteins) and the limited number of quantum calculations on S−H/π interactions beyond H_2S, which has a different geometry than typical S−H/π interactions due to the bidentate nature of its interaction with the aromatic ring. In contrast to prior investigations, the results herein include calculations based on the crystallographically determined structure of an S−H/π interaction with the hydrogen localized. S−H/π interactions have been described substantially in electrostatic (δ^+(H)·δ^-(π)), induced dipole, and dispersion terms.[2g,6b] Alternatively, Biswal and Wategaonkar described the H_2S·benzene interaction primarily via molecular orbital overlap/HOMO−LUMO-type interactions.[2h] Consistent with both electrostatic and orbital overlap explanations, more electron-rich aromatic systems exhibit stronger or more frequent S−H/π interactions, as observed by IR[6b] and by the greater frequency of Cys interactions with Trp in the PDB.[2k,6b,c,10d] More electron-rich aromatics, in addition to having more negative electrostatic potentials, exhibit an increase in their π donor molecular orbital energies, thus permitting more similar energies of the donor and acceptor orbitals. These more similar energies result in greater energetic stabilization in the interaction, in a manner comparable to orbital energy-based electronic tuning of Diels−Alder reaction rates (electron-rich diene/electron-poor dienophile, or electron-poor diene/electron-rich dienophile in inverse electron demand Diels−Alder reactions).[29]

Notably, in water and other polar solvents, where S−H/π interactions of proteins are observed,[2b,c,4a,c,10d,30] the electrostatic driving force for S−H/π interactions would be expected to be minimal, due to the small δ^+ on the thiol S−H and the presence of cations or the more significant δ^+ on the hydrogens of water. Even in the solid state, the electrostatic driving force in competitive systems should be modest, given that the partial positive charge on thiol hydrogens is similar to that of an aromatic hydrogen, suggesting that there should be minimal basis for selective S−H/π interactions in the presence of other, competitive interacting partners. Moreover, purely electrostatic arguments provide little basis for the observation of S−H···C distances that are substantially below the sum of the van der Waals radii. In contrast, molecular orbital-based interactions with the σ^* of the S−H bond would allow for the *preferential* interaction of aromatic rings with thiols, even in the presence of competitive hydrogen bond acceptors and significant competitive partial positive charges.

In considering the underlying nature of π facial interactions, analogy can be made to Pearson's hard and soft acids and bases (HSAB) principle.[31] Cation−π interactions involving alkali metals are governed by electrostatic interactions, consistent with the hard nature of the cations, the highly favorable electrostatic interactions possible via the aromatic π face, and the high energies of the available LUMOs of these cations. In contrast, π interactions with softer X−H bonds are expected to be driven by molecular orbital interactions, as was observed herein.

X−H/π interactions are often called X−H/π hydrogen bonds, in analogy to classical hydrogen bonds. In a classical hydrogen bond, the donor is the hydrogen-containing bond (e.g., an amide N−H or alcohol O−H), while the acceptor is the species containing the lone pair (e.g., from a carbonyl or alcohol O). In considering the fundamental stereoelectronic (π → σ^*) nature of S−H/π interactions suggested herein, with the π orbital functioning as the electron *donor* and the S−H σ^* orbital as the electron *acceptor*, we specifically choose to avoid using the phrase "S−H/π hydrogen bond" to describe this interaction, given the inherent reversal of roles of donor and acceptor in a proposed stereoelectronically based S−H/π interaction compared to the classical description of the hydrogen bond.

S−H/π interactions have been implied as contributors to protein stability and function in multiple analyses of the PDB. However, the absence of electron density for cysteine hydrogens in protein crystal structures has led to widely varying descriptions of the number of these interactions in the PDB.[2c,k,4a,10d,30] Analysis of ultra-high resolution structures in the PDB with the thiol hydrogen explicitly included in the structure file (only 3.8% of all structures ≤1.00 Å, emphasizing the difficulty of locating thiol hydrogens in protein crystal structures) revealed several examples of thiols interacting with aromatic rings (Figure 13). In the structure of the titin domain M7 (Figure 13a),[32] Cys79 engages in an S−H/π interaction with Trp40, with the thiol hydrogen clearly observable in the electron density map. In the structure of D-xylose isomerase (Figure 13b),[33] Cys306 is located within a cage of three aromatic residues (Phe13, Phe286, Phe288), with no traditional hydrogen bond acceptors within interaction range. In the structure of the N-terminal domain of LIP5 (Figure 13c),[34] Cys87 engages in a tight S−H/π interaction with Phe131 (2.63 Å H···$C_{aromatic}$ distance, based on the 1.20 Å S−H bond length and 109.0° C−S−H bond angle in the PDB coordinates; the H···C distance would be shorter if modeled with the more typical 1.34 Å S−H bond length and 95°−100° C−S−H bond angle). Notably, in the above (and most other) structures in the PDB with thiol hydrogens shown explicitly, the C−S−H bond angle is reported as 109.0°, which is substantially larger than typical C−S−H bond angles (∼95°−100°), and the S−H bond length 1.20 Å, also below standard S−H bond lengths. These observations suggest that additional optimization is required in the parameters and force fields for thiols, for applications in both structure determination and molecular modeling.

Viguera and Serrano observed that phenylalanine−cysteine interactions are stabilizing to α-helices when positioned with an i/i+4 relationship to each other, with up to 2.0 kcal/mol (for the Phe_i/Cys_{i+4} pair) in stabilization energy found experimentally in model α-helical peptides.[2b] Notably, in these peptides, these interactions are solvent exposed. These data

DOI: 10.1021/jacs.6b08415
J. Am. Chem. Soc. 2017, 139, 1842−1855

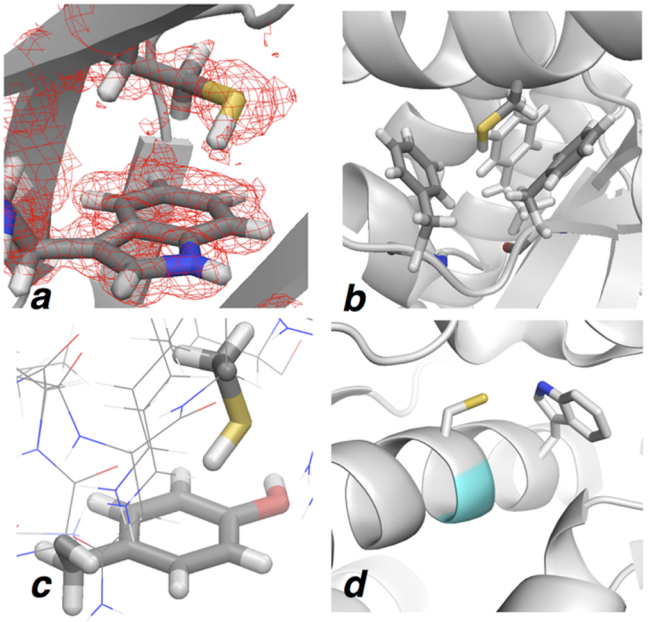

Figure 13. S−H/π interactions in the PDB. (a) Cys79−Trp40 S−H/π interaction in pdb 3puc (0.96 Å resolution), with a difference electron density map (coefficients $2F_o - F_c$) shown, that exhibits alignment of the S−H bond with the aromatic π orbital.[32] (b) Cys306 interacting in a cage of 3 phenylalanine residues in pdb 3u3h (0.97 Å resolution). The electron density map is unclear about the hydrogen position, though no traditional hydrogen bond acceptor is near the thiol.[33] (c) Cys87−Phe181 S−H/π interaction (2.63 Å H···$C_{aromatic}$ distance) in pdb 4txr (1.00 Å resolution).[34] Notably, all S−H bonds in the pdb files of panels a−c included noncanonical 1.20 Å S−H bond lengths and 109.0° C−S−H bond angles. (d) $W_{216}XXGC_{220}$ interaction within the F-helix of the protein kinase CK2 (pdb 3war, 1.04 Å resolution).[36] Gly219 is indicated in cyan.

were correlated with the high frequency of close interactions of cysteine and methionine with aromatic residues that was previously observed by Thornton.[2a] We analyzed the structures identified by Zhou et al. to exhibit cysteine−aromatic interactions, and additionally conducted a search of the Protein Geometry Database (PGD) of high resolution structures, to identify α-helical cysteine−aromatic interactions.[10d,35] Among the 23 [FYW]XXXC sequences (Cys not in a disulfide) in α-helices that were found in the PGD in structures ≤1.20 Å resolution, 17 exhibited close intrahelical interactions of Cys with the aromatic rings (S···C < 3.8 Å). Most intriguingly, the structure of the protein kinase CK2 (Figure 13d)[36] exhibited a Trp_{216}−Cys_{220} i/i+4 interaction (S···aromatic distance 3.18 Å, no hydrogens in the structure file) within an unusual α-helical sequence WSLGC that places the glycine as a central residue of a 16 residue α-helix. This helix, known as the F-helix, functions as the organizing center of protein kinase domains, interacting with both the regulatory and catalytic spines.[37] Interestingly, analysis of all human protein kinase sequences revealed that 93 protein kinases contain a WXXGC motif, which in CK2 features a Trp−Cys interaction with an intermediate glycine, with all residues in the α-helix. Protein kinases with a WXXGC motif were observed in three branches of the protein kinase tree, including 56 of 61 CMGC kinases (including Erk, JNK, GSK-3β, and most cyclin-dependent kinases), 7 MAP3Ks, the 4 polo-like kinases, 7 AGC kinases, and 17 kinases in the branches between the CMGC and CAMK kinases.[38] Twelve additional kinases contain related [FYW]XXXC motifs here, including the DNA damage-activated cell cycle checkpoint kinases ATM and ATR, which have FXXXC sequences at these positions. In total, 105 protein kinases, or 20% of the human kinome, contain an $aromatic_i$−$cysteine_{i+4}$ motif within the F-helix. In contrast, most other kinases have a large hydrophobic residue in place of Cys, which in examined structures interacts with the Trp via a hydrophobic interaction (e.g., protein kinase A, pdb 1rdq, WXXGV sequence in an α-helix, with a W−V hydrophobic interaction).[39] These sequence patterns are also observed in kinases in organisms as evolutionarily distant as yeast (WXXGC (35 kinases) or WXXG[IVL] (58 kinases) or related [aromatic]XX[AG][Cys/hydrophobic] motifs are found in 111 of 122 *S. cereviseae* protein kinases), indicating strong conservation of both the central glycine and interactions of adjacent Cys or hydrophobic residues with a Trp that is 4 residues (i.e., one α-helical turn) away within the F-helix. Notably, protein kinases are subject to redox regulation.[1,40] While a regulatory role for oxidation of this cysteine has not to our knowledge been identified, Cys oxidation here would disrupt the observed S−H/π interaction and weaken the α-helix, and could potentially function as a redox-mediated switch to change the structure and function of the protein kinase. Future work will be necessary to examine this speculative mechanism.

S−H/π interactions are one of a series of neutral X−H/π interactions, including the most thoroughly investigated C−H/π interactions.[2h,6b,d−h,16b,d] These X−H/π interactions in general are characterized by only modestly polarized X−H bonds, resulting in a weak inherent electrostatic driving force for the interactions. Despite this apparently modest electrostatic basis for these interactions, they are observed ubiquitously in crystals, in organic solvents, and in water. The results herein, which suggest an inherent stereoelectronic basis for S−H/π interactions, provide an explanation for the observation of S−H/π interactions in solution and solid-state conditions of highly divergent polarity, and could find broad application in the understanding of other related, weakly polar X−H/π interactions.

■ ASSOCIATED CONTENT

Supporting Information

The Supporting Information is available free of charge on the ACS Publications website at DOI: 10.1021/jacs.6b08415. The CIF files for **1** and **2** have been deposited with the Cambridge Crystallographic Data Centre under CCDC 1416010 and 1416011, respectively.

Crystallographic structure of **1** (CIF)
Crystallographic structure of **1** with normalized S−H bond length (CIF)
Crystallographic structure of **2** (CIF)
Table S1, Full data sets from thiol−π bond CSD search (XLS)
Table S2, Full data sets from normalized S−H bond length thiol−π bond CSD search (XLS)
Table S3, Full data sets from lithium−π bond CSD search (XLS)
Table S4, Full data sets from sodium−π bond CSD search (XLS)
Table S5, Full data sets from potassium−π bond CSD search (XLS)
Table S6, Full data sets from alcohol−π bond CSD search (XLS)

DOI: 10.1021/jacs.6b08415
J. Am. Chem. Soc. 2017, 139, 1842−1855

Table S7, Full data sets from Rb−π bond, Cs−π bond, and Ag−π bond CSD searches (XLS)
Experimental procedures, NMR spectra, X-ray crystallography data, additional IR, and computational data (PDF)

AUTHOR INFORMATION

Corresponding Authors

*zondlo@udel.edu
*sapatel@udel.edu
*gpyap@udel.edu
*bais@udel.edu

ORCID

Neal J. Zondlo: 0000-0002-7417-8085

Present Address

[§]Department of Chemistry, Indian Institute of Technology, Ropar, Rupnagar, 140001, India.

Author Contributions

[‡]S.K.S. and H.K.G. contributed equally.

Notes

The authors declare no competing financial interest.

ACKNOWLEDGMENTS

We thank NSF (1403532), NIH (GM93225), and the University of Delaware for support of this work. Instrumentation support was provided by NIH (GM110758) and NSF (CHE-1229234). We thank Joel Rosenthal for the use of IR instrumentation. We thank John Famiglietti and Moiscell Robinson for the design and construction of the modifications to the IR instrumentation to permit temperature control and measurement. We thank Brian Bahnson and Colin Thorpe for helpful discussions.

REFERENCES

(1) Paulsen, C. E.; Carroll, K. S. *Chem. Rev.* **2013**, *113*, 4633−4679.
(2) (a) Reid, K. S. C.; Lindley, P. F.; Thornton, J. M. *FEBS Lett.* **1985**, *190*, 209−213. (b) Viguera, A. R.; Serrano, L. *Biochemistry* **1995**, *34*, 8771−8779. (c) Pal, D.; Chakrabarti, P. *J. Biomol. Struct. Dyn.* **1998**, *15*, 1059−1072. (d) Zauhar, R. J.; Colbert, C. L.; Morgan, R. S.; Welsh, W. J. *Biopolymers* **2000**, *53*, 233−248. (e) Pal, D.; Chakrabarti, P. *J. Biomol. Struct. Dyn.* **2001**, *19*, 115−128. (f) Tatko, C. D.; Waters, M. L. *Protein Sci.* **2004**, *13*, 2515−2522. (g) Tauer, T. P.; Derrick, M. E.; Sherrill, C. D. *J. Phys. Chem. A* **2005**, *109*, 191−196. (h) Biswal, H. S.; Wategaonkar, S. *J. Phys. Chem. A* **2009**, *113*, 12774−12782. (i) Daeffler, K. N. M.; Lester, H. A.; Dougherty, D. A. *J. Am. Chem. Soc.* **2012**, *134*, 14890−14896. (j) Beno, B. R.; Yeung, K.-S.; Bartberger, M. D.; Pennington, L. D.; Meanwell, N. A. *J. Med. Chem.* **2015**, *58*, 4383−4438. (k) Hussain, H. B.; Wilson, K. A.; Wetmore, S. D. *Aust. J. Chem.* **2015**, *68*, 385−395. (l) Biswal, H. S.; Bhattacharyya, R.; Bhattacherjee, A.; Wategaonkar, S. *Int. Rev. Phys. Chem.* **2015**, *34*, 99−160.
(3) (a) Sencanski, M.; Dosen-Micovic, L.; Sukalovic, V.; Kostic-Rajacic, S. *Struct. Chem.* **2015**, *26*, 1139−1149. (b) Drobecq, H.; Boll, E.; Senechal, M.; Desmet, R.; Saliou, J. M.; Lacapere, J. J.; Mougel, A.; Vicogne, J.; Melnyk, O. *Bioconjugate Chem.* **2016**, *27*, 1540−1546. (c) Gomez-Tamayo, J. C.; Cordomi, A.; Olivella, M.; Mayol, E.; Fourmy, D.; Pardo, L. *Protein Sci.* **2016**, *25*, 1517−1524.
(4) (a) Ringer, A. L.; Senenko, A.; Sherrill, C. D. *Protein Sci.* **2007**, *16*, 2216−2223. (b) Leverentz, H. R.; Truhlar, D. G. *J. Phys. Chem. A* **2008**, *112*, 6009−6016. (c) Duan, G. L.; Smith, V. H.; Weaver, D. F. *Mol. Phys.* **2001**, *99*, 1689−1699. (d) Mintz, B. J.; Parks, J. M. *J. Phys. Chem. A* **2012**, *116*, 1086−1092. (e) Alberti, M.; Aguilar, A.; Huarte-Larranaga, F.; Lucas, J. M.; Pirani, F. *J. Phys. Chem. A* **2014**, *118*, 1651−1662. (f) Orabi, E. A.; English, A. M. *Isr. J. Chem.* **2016**, *56*, 872−885.
(5) (a) Hunter, C. A.; Lawson, K. R.; Perkins, J.; Urch, C. J. *J. Chem. Soc. Perkin 2* **2001**, 651−669. (b) Meyer, E. A.; Castellano, R. K.; Diederich, F. *Angew. Chem., Int. Ed.* **2003**, *42*, 1210−1250. (c) Salonen, L. M.; Ellermann, M.; Diederich, F. *Angew. Chem., Int. Ed.* **2011**, *50*, 4808−4842. (d) Ma, J. C.; Dougherty, D. A. *Chem. Rev.* **1997**, *97*, 1303−1324.
(6) (a) Saggu, M.; Levinson, N. M.; Boxer, S. G. *J. Am. Chem. Soc.* **2011**, *133*, 17414−17419. (b) Saggu, M.; Levinson, N. M.; Boxer, S. G. *J. Am. Chem. Soc.* **2012**, *134*, 18986−18997. (c) Steiner, T.; Koellner, G. *J. Mol. Biol.* **2001**, *305*, 535−557. (d) Nishio, M.; Hirota, M. *Tetrahedron* **1989**, *45*, 7201−7245. (e) Nishio, M.; Hirota, M.; Umezawa, Y. *CH/π Interaction: Evidence, Nature, and Consequences*; Wiley & Sons: New York, 1998. (f) Nishio, M. *CrystEngComm* **2004**, *6*, 130−158. (g) Takahashi, O.; Kohno, Y.; Nishio, M. *Chem. Rev.* **2010**, *110*, 6049−6076. (h) Nishio, M.; Umezawa, Y.; Fantini, J.; Weiss, M. S.; Chakrabarti, P. *Phys. Chem. Chem. Phys.* **2014**, *16*, 12648−12683.
(7) (a) Forbes, C. R.; Zondlo, N. J. *Org. Lett.* **2012**, *14*, 464−467. (b) Zondlo, N. J. *Acc. Chem. Res.* **2013**, *46*, 1039−1049. (c) Pandey, A. K.; Thomas, K. M.; Forbes, C. R.; Zondlo, N. J. *Biochemistry* **2014**, *53*, 5307−5314.
(8) Forbes, C. R.; Pandey, A. K.; Ganguly, H. K.; Yap, G. P. A.; Zondlo, N. J. *Org. Biomol. Chem.* **2016**, *14*, 2327−2346.
(9) Sawada, N.; Itoh, T.; Yasuda, N. *Tetrahedron Lett.* **2006**, *47*, 6595−6597.
(10) (a) Rozenberg, M. S.; Nishio, T.; Steiner, T. *New J. Chem.* **1999**, *23*, 585−586. (b) Vangala, V. R.; Desiraju, G. R.; Jetti, R. K. R.; Bläser, D.; Boese, R. *Acta Crystallogr., Sect. C: Cryst. Struct. Commun.* **2002**, *C58*, o635−o636. (c) Dolega, A.; Marynowski, W.; Baranowska, K.; Smiechowski, M.; Stangret, J. *Inorg. Chem.* **2012**, *51*, 836−843. (d) Zhou, P.; Tian, F.; Lv, F.; Shang, Z. *Proteins: Struct., Funct., Genet.* **2009**, *76*, 151−163.
(11) Gilli, G.; Gilli, P. *The Nature of the Hydrogen Bond: Outline of a Comprehensive Hydrogen Bond Theory*; Oxford University Press: New York, 2009.
(12) Alauddin, M.; Biswal, H. S.; Gloaguen, E.; Mons, M. *Phys. Chem. Chem. Phys.* **2015**, *17*, 2169−2178.
(13) (a) Antinolo, A.; Fernandez-Galan, R.; Molina, N.; Otero, A.; Rivilla, I.; Rodriguez, A. M. *Inorg. Chim. Acta* **2010**, *363*, 3489−3497. (b) Bicca de Alencastro, R.; Sandorfy, C. *Can. J. Chem.* **1972**, *50*, 3594−3600.
(14) (a) David, J. G.; Hallam, H. E. *Trans. Faraday Soc.* **1964**, *60*, 2013−2016. (b) Becker, B.; Felcyn, E. W.; Herman, A.; Pikies, J.; Wojnowski, W. *Z. Anorg. Allg. Chem.* **1982**, *488*, 229−234. (c) Mielcarek, A.; Dolega, A. *J. Mol. Struct.* **2016**, *1103*, 217−223.
(15) (a) Plevin, M. J.; Bryce, D. L.; Boisbouvier, J. *Nat. Chem.* **2010**, *2*, 466−471. (b) Singh, C.; Rai, R. K.; Aussenac, F.; Sinha, N. *J. Phys. Chem. Lett.* **2014**, *5*, 4044−4048.
(16) (a) Cheney, B. V.; Schulz, M. W.; Cheney, J. *Biochim. Biophys. Acta, Protein Struct. Mol. Enzymol.* **1989**, *996*, 116−124. (b) Malone, J. F.; Murray, C. M.; Charlton, M. H.; Docherty, R.; Lavery, A. J. *J. Chem. Soc., Faraday Trans.* **1997**, *93*, 3429−3436. (c) Hermida-Ramoń, J. M.; Cabaleiro-Lago; Rodriguez-Otero, J. *J. Chem. Phys.* **2005**, *122*, 204315. (d) Sherrill, C. D.; Takatani, T.; Hohenstein, E. G. *J. Phys. Chem. A* **2009**, *113*, 10146−10159.
(17) (a) Reed, A. E.; Curtiss, L. A.; Weinhold, F. *Chem. Rev.* **1988**, *88*, 899−926. (b) Glendening, C. R.; Landis, C. R.; Weinhold, F. *WIREs Comput. Mol. Sci.* **2012**, *2*, 1−42.
(18) Valley, C. C.; Cembran, A.; Perlmutter, J. D.; Lewis, A. K.; Labello, N. P.; Gao, J.; Sachs, J. N. *J. Biol. Chem.* **2012**, *287*, 34979−34991.
(19) Steiner, T. *Angew. Chem., Int. Ed.* **2002**, *41*, 48−76.
(20) Allen, F. H. *Acta Crystallogr., Sect. B: Struct. Sci.* **2002**, *B58*, 380−388.
(21) Interactions of Rb^+ and Cs^+ exhibit evidence of covalent character in the bonds to aromatic systems, including puckering of the aromatic ring (ref 22e) in a manner analogous to η^1-interactions of transition metals with arenes.

DOI: 10.1021/jacs.6b08415
J. Am. Chem. Soc. 2017, 139, 1842−1855

(22) (a) Sunner, J.; Nishizawa, K.; Kebarle, P. *J. Phys. Chem.* **1981**, *85*, 1814−1820. (b) Dougherty, D. A. *Science* **1996**, *271*, 163−168. (c) Mecozzi, S.; West, A. P.; Dougherty, D. A. *Proc. Natl. Acad. Sci. U. S. A.* **1996**, *93*, 10566−10571. (d) Mecozzi, S.; West, A. P.; Dougherty, D. A. *J. Am. Chem. Soc.* **1996**, *118*, 2307−2308. (e) Fukin, G. K.; Lindeman, S. V.; Kochi, J. K. *J. Am. Chem. Soc.* **2002**, *124*, 8329−8336. (f) Abraham, S. A.; Jose, D.; Datta, A. *ChemPhysChem* **2012**, *13*, 695−698. (g) Mahadevi, A. S.; Sastry, G. N. *Chem. Rev.* **2013**, *113*, 2100−2138. (h) Dougherty, D. A. *Acc. Chem. Res.* **2013**, *46*, 885−893.
(23) (a) Hubig, S. M.; Lindeman, S. V.; Kochi, J. K. *Coord. Chem. Rev.* **2000**, *200*, 831−873. (b) Lindeman, S. V.; Rathore, R.; Kochi, J. K. *Inorg. Chem.* **2000**, *39*, 5707−5716. (c) Zaric, S. D. *Eur. J. Inorg. Chem.* **2003**, *2003*, 2197−2209. (d) Guerrero, A.; Martin, E.; Hughes, D. L.; Kaltsoyannis, N.; Bochmann, M. *Organometallics* **2006**, *25*, 3311−3313. (e) Herrero-Gomez, E.; Nieto-Oberhuber, C.; Lopez, S.; Benet-Buchholz, J.; Echavarren, A. M. *Angew. Chem., Int. Ed.* **2006**, *45*, 5455−5459. (f) Habata, Y.; Ikeda, M.; Yamada, S.; Takahashi, H.; Ueno, S.; Suzuki, T.; Kuwahara, S. *Org. Lett.* **2012**, *14*, 4576−4579. (g) Falceto, A.; Carmona, E.; Alvarez, S. *Organometallics* **2014**, *33*, 6660−6668. (h) Liang, M. X.; Ruan, C. Z.; Sun, D.; Kong, X. J.; Ren, Y. P.; Long, L. S.; Huang, R. B.; Zheng, L. S. *Inorg. Chem.* **2014**, *53*, 897−902.
(24) (a) Zheng, J. R.; Kwak, K.; Asbury, J.; Chen, X.; Piletic, I. R.; Fayer, M. D. *Science* **2005**, *309*, 1338−1343. (b) Zheng, J. R.; Fayer, M. D. *J. Am. Chem. Soc.* **2007**, *129*, 4328−4335. (c) Rosenfeld, D. E.; Gengeliczki, Z.; Fayer, M. D. *J. Phys. Chem. B* **2009**, *113*, 13300−13307. (d) Nikolova, V.; Ilieva, S.; Galabov, B.; Schaefer, H. F. *J. Org. Chem.* **2014**, *79*, 6823−6831.
(25) Graton, J.; Besseau, F.; Brossard, A. M.; Charpentier, E.; Deroche, A.; Le Questel, J. Y. *J. Phys. Chem. A* **2013**, *117*, 13184−13193.
(26) (a) Escher, E.; Bernier, M.; Parent, P. *Helv. Chim. Acta* **1983**, *66*, 1355−1365. (b) Hobbs, D. W.; Still, W. C. *Tetrahedron Lett.* **1987**, *28*, 2805−2808. (c) Lu, H. S. M.; Volk, M.; Kholodenko, Y.; Gooding, E.; Hochstrasser, R. M.; DeGrado, W. F. *J. Am. Chem. Soc.* **1997**, *119*, 7173−7180. (d) Gao, R.; Zhang, Y.; Choudhury, A. K.; Dedkova, L. M.; Hecht, S. M. *J. Am. Chem. Soc.* **2005**, *127*, 3321−3331. (e) Chen, S. X.; Zhang, Y.; Hecht, S. M. *Biochemistry* **2011**, *50*, 9340−9351. (f) Rudolf, J. D.; Poulter, C. D. *ACS Chem. Biol.* **2013**, *8*, 2707−2714.
(27) Gellman, S. H. *Biochemistry* **1991**, *30*, 6633−6636.
(28) (a) Voth, A. R.; Khuu, P.; Oishi, K.; Ho, P. S. *Nat. Chem.* **2009**, *1*, 74−79. (b) Wilcken, R.; Zimmermann, M. O.; Lange, A.; Joerger, A. C.; Boeckler, F. M. *J. Med. Chem.* **2013**, *56*, 1363−1388.
(29) Sauer, J.; Sustmann, R. *Angew. Chem., Int. Ed. Engl.* **1980**, *19*, 779−807.
(30) Brandl, M.; Weiss, M. S.; Jabs, A.; Sühnel, J.; Hilgenfeld, R. *J. Mol. Biol.* **2001**, *307*, 357−377.
(31) Pearson, R. G. *J. Am. Chem. Soc.* **1963**, *85*, 3533−3539.
(32) Sauer, F.; Vahokoski, J.; Song, Y. H.; Wilmanns, M. *EMBO Rep.* **2010**, *11*, 534−540.
(33) Toteva, M. M.; Silvaggi, N. R.; Allen, K. N.; Richard, J. P. *Biochemistry* **2011**, *50*, 10170−10181.
(34) Vild, C. J.; Li, Y.; Guo, E. Z.; Liu, Y.; Xu, Z. H. *J. Biol. Chem.* **2015**, *290*, 7291−7303.
(35) Berkholz, D. S.; Krenesky, P. B.; Davidson, J. R.; Karplus, P. A. *Nucleic Acids Res.* **2010**, *38*, D320−D325.
(36) Schulze Gahmen, U.; De Bondt, H. L.; Kim, S. H. *J. Med. Chem.* **1996**, *39*, 4540−4546.
(37) (a) Kornev, A. P.; Taylor, S. S.; Ten Eyck, L. F. *Proc. Natl. Acad. Sci. U. S. A.* **2008**, *105*, 14377−14382. (b) Taylor, S. S.; Kornev, A. P. *Trends Biochem. Sci.* **2011**, *36*, 65−77.
(38) Manning, G.; Whyte, D. B.; Martinez, R.; Hunter, T.; Sudarsanam, S. *Science* **2002**, *298*, 1912−1934.
(39) Yang, J.; Ten Eyck, L. F.; Xuong, N.-H.; Taylor, S. S. *J. Mol. Biol.* **2004**, *336*, 473−487.
(40) Klomsiri, C.; Karplus, P. A.; Poole, L. B. *Antioxid. Redox Signaling* **2011**, *14*, 1065−1077.
(41) See the Supporting Information for details.
(42) Ballmann, J.; Fuchs, M. G. G.; Dechert, S.; John, M.; Meyer, F. *Inorg. Chem.* **2009**, *48*, 90−99.
(43) Hiller, W.; Rundel, W. *Acta Crystallogr., Sect. C: Cryst. Struct. Commun.* **1993**, *49*, 1127−1128.
(44) Döring, A.; Fischer, C.; Schulzke, C. *Z. Anorg. Allg. Chem.* **2013**, *639*, 1552−1558.
(45) Hildebrand, A.; Loennecke, P.; Silaghi-Dumitrescu, L.; Hey-Hawkins, E. *Dalton Trans.* **2008**, 4639−4646.
(46) Bernardinelli, G.; Geoffroy, M.; Franzi, R. *Z. Kristallogr.* **1991**, *195*, 147−149.
(47) (a) Lipschutz, M. I.; Tilley, T. D. *Angew. Chem., Int. Ed.* **2014**, *53*, 7290−7294. (b) Wooles, A. J.; Lewis, W.; Blake, A. J.; Liddle, S. T. *Organometallics* **2013**, *32*, 5058−5070. (c) Knepper, I.; Seichter, W.; Skobridis, K.; Theodorou, V.; Weber, E. *CrystEngComm* **2015**, *17*, 6355−6369. (d) Goy, R.; Bertini, L.; Elleouet, C.; Görls, H.; Zampella, G.; Talarmin, J.; De Gioia, L.; Schollhammer, P.; Apfel, U.-P.; Weigand, W. *Dalton Trans.* **2015**, *44*, 1690−1699. (e) Valencia, L.; Adams, H.; Bastida, R.; Fenton, D. E.; Macías, A. *Inorg. Chim. Acta* **2001**, *317*, 45−52.

DOI: 10.1021/jacs.6b08415
J. Am. Chem. Soc. 2017, 139, 1842−1855